Strain-Tunable Single Photon Sources in WSe₂ Monolayers

Oliver Iff,[†,○] Davide Tedeschi,[‡,○] Javier Martín-Sánchez,[*,§,∥,○] Magdalena Moczała-Dusanowska,[†] Sefaattin Tongay,[⊥] Kentaro Yumigeta,[⊥] Javier Taboada-Gutiérrez,[§,∥] Matteo Savaresi,[‡] Armando Rastelli,[#] Pablo Alonso-González,[§,∥] Sven Höfling,[†,∇] Rinaldo Trotta,[*,‡] and Christian Schneider[*,†]

[†]Technische Physik and Wilhelm Conrad Röntgen Research Center for Complex Material Systems, Physikalisches Institut, Universität Würzburg, Am Hubland, D-97074 Würzburg, Germany
[‡]Department of Physics, Sapienza University of Rome, Piazzale A. Moro 5, 00185 Rome, Italy
[§]Department of Physics, University of Oviedo, Oviedo, Spain
[∥]Center of Research on Nanomaterials and Nanotechnology, CINN (CSIC−Universidad de Oviedo), El Entrego 33940, Spain
[⊥]Arizona State University, Glendale, Arizona 85306, United States
[#]Institute of Semiconductor and Solid State Physics, Johannes Kepler University Linz, Altenbergerstraße 69, 4040 Linz, Austria
[∇]SUPA, School of Physics and Astronomy, University of St. Andrews, St. Andrews, KY16 9SS, United Kingdom

ⓢ *Supporting Information*

ABSTRACT: The appearance of single photon sources in atomically thin semiconductors holds great promises for the development of a flexible and ultracompact quantum technology in which elastic strain engineering can be used to tailor their emission properties. Here, we show a compact and hybrid two-dimensional semiconductor-piezoelectric device that allows for controlling the energy of single photons emitted by quantum emitters localized in wrinkled WSe₂ monolayers. We demonstrate that strain fields exerted by the piezoelectric device can be used to tune the energy of localized excitons in WSe₂ up to 18 meV in a reversible manner while leaving the single photon purity unaffected over a wide range. Interestingly, we find that the magnitude and, in particular, the sign of the energy shift as a function of stress is emitter dependent. With the help of finite element simulations we suggest a simple model that explains our experimental observations and, furthermore, discloses that the type of strain (tensile or compressive) experienced by the quantum emitters strongly depends on their localization across the wrinkles. Our findings are of strong relevance for the practical implementation of single photon devices based on two-dimensional materials as well as for understanding the effects of strain on their emission properties.

KEYWORDS: *single photon emitters, 2D materials, elastic strain engineering, photoluminescence, tungsten diselenide monolayers, piezoelectric devices*
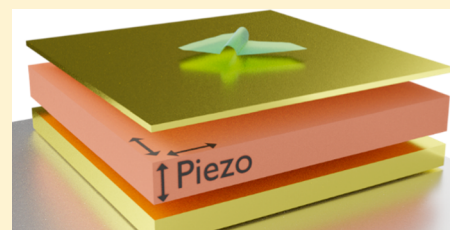
The family of two-dimensional (2D) semiconductor transition metal dichalcogenides (TMDs), including WS₂, WSe₂, MoS₂, or MoSe₂, offers several advantages for optoelectronic and photonic applications. They feature a variety of properties such as direct bandgap when thinned down to the monolayer, quantum confinement due to their reduced out-of-plane dimensionality, large oscillator strength and quantum efficiency, optically controlled injection of electrons with defined spins for quantum spintronics and spin-photon interfacing.[1,2] Moreover, functional multilayer heterostructures can be easily built by piling up one material on top of the other—not possible by conventional epitaxial growth techniques—and ultracompact optoelectronic devices such as light emitting diodes have been already fabricated.[3] Another major advantage of 2D materials compared to conventional semiconductors is their impressive "stretchability", as they can withstand strain magnitudes well above 1%

before mechanical rupture takes place. This offers a large playground for elastic strain engineering since externally applied strain—by direct bending or using piezoelectric actuators[4−9]—provides a natural strategy to tailor the electronic and optical properties of the material.

The discovery of single photon emitters (SPEs) in 2D materials has stimulated an intensive research effort, aimed at the exploitation of such sources for quantum photonics[10] as well as at the understanding of their physical origin. In the last years, SPEs have been reported on TMD monolayers at cryogenic temperatures[11−15] and on layered hexagonal boron nitride up to room temperature.[16] The origin of SPEs has been attributed to either presence of defects in the crystalline
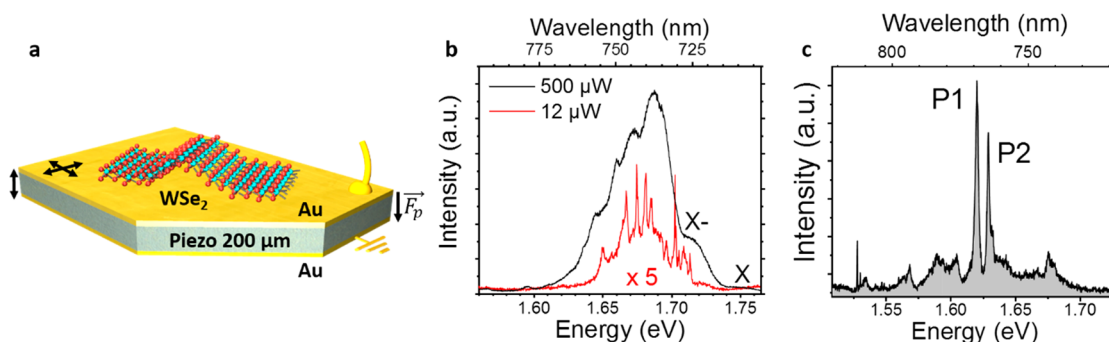
Figure 1. (a) Schematics of a hybrid 2D-semiconductor-piezoelectric actuator with an integrated WSe$_2$ monolayer. (b) Typical microphotoluminescence spectrum of a WSe$_2$ monolayer, including the exciton (X) and the trion (X-), which breaks up at low pump power into discrete emission lines in the spectral range around 725−780 nm. (c) Close up spectrum of a pair of selected lines P1 and P2 with a line width of about 230 μeV.

structure of the crystals[16,17] or bandgap modulation of the material due to local bending of the material itself, which naturally occurs on bubbles or wrinkles.[18] In an attempt to realize scalable SPEs over large areas, quantum dot-like nanostructures have been fabricated in atomically thin WSe$_2$ or WS$_2$ bilayers and monolayers by local strain engineering: predefined areas of the monolayer were elastically deformed by pillars or nanorods.[19−21] A recent theoretical work has suggested that this deformation induces the confinement of excitons in potential wells with bound states that might lead to emission of single photons.[18] First attempts to couple WSe$_2$ quantum emitters to optical resonances of metallic nanostructures[22−25] and waveguide structures[26,27] have also been reported, which outlines the possibility for integration of TMD monolayers with optical cavities and on-chip integrated quantum photonic circuits.

In spite of these significant advances, quantum emitters in 2D materials deliver photons at random energies, which are difficult to control owing to the complexity either of the potential profile eventually leading to the exciton confinement or to the nature of the defects. In turn, this severely limits the suitability of 2D SPEs for applications in quantum information science and technology. Therefore, it is fundamental to develop postfabrication tuning methods capable of controlling the SPEs emission energy in a reversible manner while leaving their optical quality unaffected. Elastic strain engineering of the material's band structure is a promising strategy to accomplish this task, as previously demonstrated on self-assembled III−V quantum dots.[28,29] Previous results on defect-induced emitters in thick hBN flakes reported moderate shift values of about 6 meV/%, likely due to the poor strain transfer efficiency of the substrate-bending technique used in the experiments.[30] To the best of our knowledge, no systematic and comprehensive studies on the strain effects in TMDs, including the impact on the single photon purity in SPEs, have been reported until now.

In this work, we successfully demonstrate active tuning of the emission energy of SPEs in WSe$_2$ monolayers using (001)- and (110)- [Pb(Mg$_{1/3}$Nb$_{2/3}$)O$_3$]$_{0.72}$-[PbTiO$_3$]$_{0.28}$ (PMN−PT) piezoelectric actuators. We show that a reversible tuning range of up to 18 meV can be obtained for moderate applied electric fields of about 15 kV/cm and that the single photon purity—as measured via the second order correlation function—is unaffected by strain, with a value g$^{(2)}$(0) bound to ∼0.12 over a range of 5 meV. Interestingly, we find that upon the same applied voltage, different quantum emitters show

completely different energy-shifts, both in magnitude and sign. Using finite element calculations, we discuss that this effect can be attributed to a different location of the quantum emitters across a wrinkle, which "feel" different strain fields (tensile and compressive) for the same induced strain field delivered by the piezo-actuator.

We first study the possibility of implementing a hybrid 2D-WSe$_2$-piezoelectric device capable of delivering single photons with controlled energy. Figure 1a shows a sketch of our device: a wrinkled WSe$_2$ monolayer obtained by mechanical exfoliation is transferred on top of a PMN−PT piezoelectric plate coated with a Cr (3 nm)/Au (100 nm) bilayer on both sides for electrical contact.[31] In a final step, the full device is mounted onto an AlN chip carrier providing electrical contacts. The application of an electric field along the poling direction of the piezoelectric actuator (F$_p$) produces an out-of-plane deformation of the plate, which induces an in-plane deformation to the attached monolayer, as sketched in Figure 1a. In particular, a positive (negative) electric field leads to a compressive (tensile) in-plane deformation of the piezo-crystal, which is transferred to the attached WSe$_2$ monolayer. Spatially resolved optical spectroscopy was performed in a microphotoluminescence (μPL) setup. The samples were excited nonresonantly at 632.8 nm in an optical cryostat. Figure 1b shows a representative photoluminescence spectrum from a WSe$_2$ monolayer at a nominal sample temperature of 5 K. At elevated pump powers, the spectrum features a characteristic line-shape revealing luminescence from the 2D exciton (X) and trion (X-) resonances, as well as a broad, structured peak spanning over the spectral range from 730 nm up to 770 nm widely attributed to quantum emitters localized in strained areas related to bubbles or wrinkles.[18,19,22,23] Atomic force microscopy (AFM) images of representative wrinkles in the monolayer are shown in Figure S1 (Supporting Information). We could identify a variety of emission lines at low excitation power, which are spectrally well-isolated and characterized by emission line width on the order of 200 μeV (see Figure 1c). We will refer hereafter to SPEs localized on wrinkled areas of the monolayer.

Spectral control over one of the observed quantum emitters is demonstrated by sweeping the electric field across to the piezoelectric actuator from F$_p$ = −20 kV/cm to F$_p$ = 20 kV/cm as shown in Figure 2a. Specifically for this emitter, an emission energy blue/red shift is observed for compressive/tensile strain fields introduced by the actuator, which is attributed to an increase/decrease of the bandgap in crystalline semiconductor
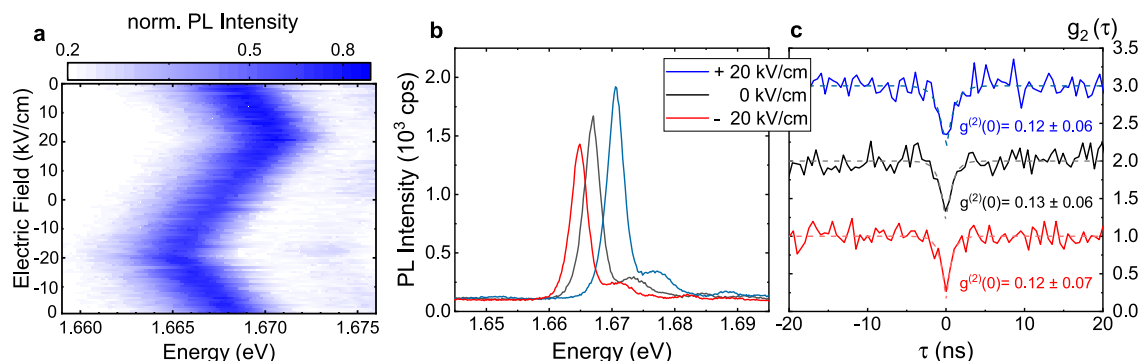
Figure 2. (a) Contour plot of the μPL spectra of a SPE as a function of the applied electric field on the piezoelectric actuator. The electric field is reversibly swept in the range from −20 to 20 kV/cm. The observed red- and blue-shifts are due to the induced compressive and tensile strain fields by the actuator. An energy shift equal to 5.4 μeV/V is observed. (b) PL spectra of the SPE in panel (a) for zero and the maximum electric fields applied on the actuator (red and blue lines). A total shift of 5.4 meV is obtained for a total field variation of 40 kV/cm. (c) Second order autocorrelation $g^{(2)}(\tau)$ measurements of the emission in panel (a) for F_p = −20, 0, and 20 kV/cm. The SPE nature is confirmed by the low deconvoluted value $g^{(2)}(0) \approx 0.12$, 0.13, and 0.12, respectively, which is independent of the applied field (i.e., induced strain field).

materials. Moreover, the shift of the emission can be reversibly tuned in a linear fashion, as in principle expected for moderate magnitudes of the strain delivered by the piezo-actuator (see below). From a linear fit to the measured spectra, we can infer a total energy shift of about 5 meV with a ratio of 5.4 μeV/V, similar to the values reported in semiconductor nano-membranes containing quantum dots.[32] Based on previous experiments, we estimate an in-plane biaxial strain value of about 0.15% for the maximally applied electric field.[32] It should be mentioned that, due to the Gaussian-like geometry of the wrinkle in the WSe$_2$ monolayer, the induced strain magnitude and sign strongly depend on the specific SPE under investigation, as discussed in detail below.

Whether single photons with high purity can be emitted at selected energies is further studied by second order correlation measurements. To do so, we investigate the influence of induced strain fields on the spectral shape and quality of the single photon emission as seen in Figure 2b and c. The luminescence is spectrally filtered by passing through a monochromator with 0.3 nm bandwidth and coupled to a fiber connected Hanbury Brown and Twiss (HBT) setup. The HBT setup is equipped with two avalanche photodiodes (time jitter of about 400 ps) connected to the correlation electronics. Notably, we observe a well-pronounced antibunching signal at zero delay times ($\tau = 0$), allowing us to extract a deconvoluted $g^{(2)}(0)$ value of ∼0.13[33] at F_p = 0 kV/cm and 0.12 at both positive and negative F_p = 20 kV/cm. From the single exponential decay of the correlation functions, which were measured in the nonsaturation regime of the exciton, we can furthermore estimate the spontaneous emission lifetimes of the exciton with a value of about 1.0 ns, which is on the faster end of previously reported values.[11] Importantly, both the exciton lifetime, as well as the single photon purity of the emitter are fully retained in the presence of mechanical stress, as evidenced by the comparative plot in Figure 2c. This unambiguously confirms that strain does not alter the quality of the single photons emitted by quantum emitters in monolayers, at least for the strain magnitudes and anisotropy investigated in this work.

As mentioned above, different SPEs lines show different shifts as the electric field is applied to the piezo-actuator. As an example, Figure 3a shows sharp emission lines originating from another wrinkle, which exhibit red and blue shifts as the

electric field is varied from F_p = 0 to 15 kV/cm. At first sight, this is surprising since a blue shift of all the lines is expected for compressive strain delivered by the actuator. In order to explain this peculiar finding, it is first important to note that light is collected over a region with a diameter of ∼1 μm, and therefore, the whole wrinkle is probed in the experiment. Second, previous reports[16,17,19] have shown that SPEs are likely related to the presence of defects in the monolayer, whose luminescence intensity is enhanced by strain fields via the funnel effect. It is therefore reasonable to assume that the different lines originate from different regions of the wrinkle where the initial strain distribution and its variation with the externally applied stress may be completely different. To support this hypothesis, we perform finite element simulations (FEM) of the strain field distribution in a WSe$_2$ flake featuring a representative Gaussian-shaped wrinkle subject to a deformation induced by a piezoelectric actuator. Details about the simulations can be found in the Supporting Information. Although each wrinkle is slightly different, we simulate a wrinkle with dimensions 100 nm (width) and 40 nm (height) and around 1.5 μm (length) in agreement with AFM measurements (see Figure S1 in Supporting Information). The WSe$_2$ flake is simulated as a continuum film with thickness of 0.7 nm. Figure 3b shows the hydrostatic strain distribution map $\varepsilon_{xx} + \varepsilon_{yy} + \varepsilon_{zz}$ (directly connected to the energy shift via the materials' deformation potentials) for a specific electric field F_p = 30 kV/cm applied on a (001)−PMN-PT piezoelectric actuator, which has an isotropic piezoelectric response, i.e., nominally isotropic biaxial in-plane strain fields are delivered by this kind of plates. It should be noted that the strain map reported in panel (b) is not the absolute strain configuration of the wrinkle, but its variation upon the application of an electric field F_p=30 kV/cm. Hence, this map represents only the induced strain field on the wrinkle, and its initial prestress configuration, since unknown, is not taken into account in the FEM simulation. As expected, a uniform compressive strain distribution is obtained on the flat areas of the monolayer in contact with the piezoelectric actuator (e.g. point D in Figure 3b), whereas a highly nonuniform strain field distribution is obtained in the suspended wrinkle. Most interestingly, the sign of the strain (tensile or compressive) strongly depends on the specific location across the wrinkle with a gradual increase of the magnitude for compressive strain
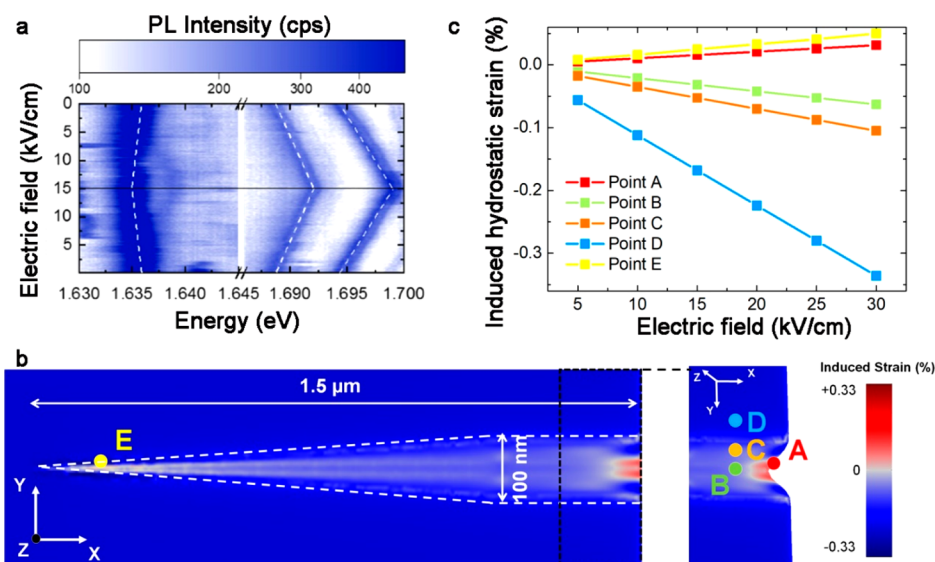
Figure 3. (a) Contour plot of the PL spectra of SPEs as a function of the electric field applied on a (001) piezoelectric device. The electric field was set up to F_p = 15 kV/cm and back to F_p= 0 kV/cm. The black line in the middle highlights the point where the maximum voltage is applied. Three different peaks can be followed along the voltage sweep, two of which show a large blue-shift (6 meV), while the other one exhibits a small red-shift (1 meV). It is worth noting the absence of any kind of hysteresis along the voltage cycle on all the energy shifts. (b) FEM simulation of the hydrostatic strain exerted over a wrinkle on a (001) piezoelectric actuator, biased at an electric field of F_p = 30 kV/cm. A triangular shape in the x-y plane and a Gaussian profile with an aspect ratio of 2.5 in the y-z cross-section are assumed as geometrical shape for the wrinkle in agreement with the AFM characterization (see Figure S1 in Supporting Information). Both compressive and tensile strain fields are observed at different positions on the wrinkle upon application of the electric field to the piezoelectric device. (c) Evolution of the hydrostatic strain as a function of the electric field applied to a (001) piezoelectric device calculated in five different points of the wrinkle, highlighted also in panel (b). Independently of the type of strain, a linear dependence with the applied voltage is observed.
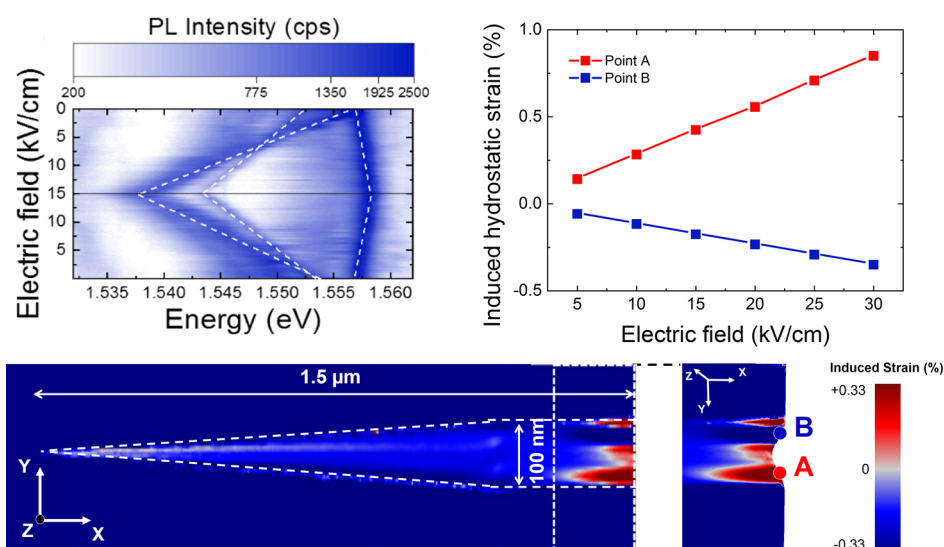

Figure 4. (a) Contour plot of the PL spectra of SPEs as a function of the electric field applied on a (110) piezoelectric device. The electric field was set up to F_p = 15 kV/cm and back to F_p= 0 kV/cm. The black line in the middle highlights the point where the maximum voltage is applied. Three different peaks can be followed along the voltage sweep, among which two show a very large red-shift (up to 18 meV), while the other one exhibits a small red-shift (1 meV). (b) FEM simulation of the hydrostatic strain exerted over the wrinkle on a (110) piezoelectric actuator, biased at an electric field of F_p = 30 kV/cm. The same geometry as in Figure 3b was used. Both compressive and tensile strain fields are observed at different positions on the wrinkle upon application of the electric field to the piezoelectric device. (c) Evolution of the hydrostatic strain as a function of the electric field applied to the piezoelectric device calculated in two different points of the wrinkle, highlighted also in panel (b).

as we move from the top to the tail (points B to D in Figure 3b). However, for the wrinkle geometry studied here, tensile strain is found at specific positions at the edges of the wrinkle (points A and B). Moreover, also the slope strain/electric field is position dependent as shown in Figure 3c), with relatively small values for tensile and large values for compressive strain. While the comparison between theory and experiment would suggest that the lines red-shifting (blue-shifting) originate from the edges (body) of the wrinkle, this behavior strongly depends on the specific geometry of the wrinkle and/or the type of strain delivered by the piezoelectric actuator (see Supporting Information). To support this

statement we performed additional experiments using a (110)−PMN-PT piezoelectric plate, which nominally provides highly anisotropic in-plane strain fields ($\varepsilon_{xx} \approx -0.3\varepsilon_{yy}$), where "$x$" and "$y$" directions correspond to [100] and [01−1] crystallographic directions of the PMN−PT crystal, respectively.[34] Interestingly, exactly the opposite behavior is observed in this case as shown in Figure 4a, with a smaller blue-shift for the line at high energy and a remarkably large red-shift up to 18 meV for the lower energy lines (for a maximum electric field F_p = 15 kV/cm applied to the actuator). It should be mentioned that due to the relatively high strain anisotropy introduced by (110)-oriented piezoelectric plates, a completely different strain distribution on the wrinkle is to be expected. This is demonstrated by FEM simulations in Figure 4b, where the hydrostatic strain map for a Gaussian-shaped wrinkle with respect to the [100] direction of the piezoelectric plate is shown. We note that our experimental observations reported in Figure 4a are compatible with a situation where the emitters are located at the edge of a wrinkle (points A and B in Figure 4b). Interestingly, in this case, a large/small tensile/compressive strain field is obtained, which may explain our findings (Figure 4c). We emphasize once more the importance of the initial geometry of the wrinkle, and additional experiments are needed to clarify whether there is tight connection between strain-slope and position of the emitter. While we leave this point to future studies, it is worth emphasizing that our findings are compatible with a scenario of ref 17 (in which multiple SPEs are located at different points of the wrinkle) but not fully consistent with the idea that quantum emitters are solely located on the regions with a significant bending.[18]

In summary, we have demonstrated active control of the energy emission of SPEs localized in a wrinkled WSe$_2$ monolayer. This is achieved developing a hybrid 2D-piezoelectric device where in-plane biaxial strain fields up to a magnitude of ~0.15% can be transferred to SPEs without degrading their optical quality. We demonstrate a record tunability up to 18 meV—much larger than the best reported values in 2D materials.[30] Moreover, the SPEs retain a high-purity single photon emission upon the introduction of strain fields, as shown by time-correlation measurements.[28] Finally, we have observed that different SPEs located in the same wrinkle shift to both higher and lower energies for the same applied stress. FEM simulations suggest that this peculiar behavior is related to the specific location of the SPEs and to the high nonuniform strain distribution across the wrinkle. The results reported in this work pave the way toward the exploitation of energy-tunable SPEs and emitters of entangled photon pairs[35] based on two-dimensional crystals, and it will stimulate the use of strain-fields to understand the origin of SPEs in 2D materials. For this last point, we anticipate that anisotropic strain fields delivered by micromachined piezoelectric actuators[28,36] on 2D materials incorporated in dielectric carrier membranes[37] will have a key role.

ASSOCIATED CONTENT

Ⓢ Supporting Information

The Supporting Information is available free of charge on the ACS Publications website at DOI: 10.1021/acs.nano-lett.9b02221.

AFM of exfoliated WSe$_2$ monolayer on top of piezoelectric devices, FEM simulations, FEM simulations of alternative wrinkles' geometries, and μ-PL spectra for strained wrinkles (PDF)

AUTHOR INFORMATION

Corresponding Authors
*E-mail: christian.schneider@physik.uni-wuerzburg.de.
*E-mail: rinaldo.trotta@uniroma1.it.
*E-mail: javiermartin@uniovi.es.

ORCID Ⓘ
Oliver Iff: 0000-0002-3613-8605
Magdalena Moczała-Dusanowska: 0000-0002-8023-4290
Sefaattin Tongay: 0000-0001-8294-984X

Author Contributions
○These authors (O.I., D.T., and J.M.-S.) contributed equally to this work. J.M.-S., R.T. and C.S. conceived and supervised the experiments. O.I., D.T., M.S. and M.M.-D. performed the optical characterizations with the help of R.T. and C.S. O.I., J.M.-S. and J.T.-G. fabricated the devices. O.I., D.T., J.M.-S., A.R., P.A.-G., S.H., R.T. and C.S. performed the analysis of the results. O.I. and J.M.-S. wrote the manuscript with inputs from R.T. and C.S. J.M.-S. performed the FEM simulations with the help of R.T. and P.A.-G. S.T. and K.Y. performed the growth of the WSe$_2$ crystals.

Notes
The authors declare no competing financial interest.

REFERENCES

(1) Kolobov, A. V.; Tominaga, J. Two-Dimensional Transition-Metal Dichalcogenides. *Springer Ser. Mater. Sci.* **2016**, *239*, 227.
(2) Liu, G.-B.; Pang, H.; Yao, Y.; Yao, W. Intervalley Coupling by Quantum Dot Confinement Potentials in Monolayer Transition Metal Dichalcogenides. *New J. Phys.* **2014**, *16*, 105011.
(3) Withers, F.; Del Pozo-Zamudio, O.; Mishchenko, A.; Rooney, a. P.; Gholinia, A.; Watanabe, K.; Taniguchi, T.; Haigh, S. J.; Geim, a. K.; Tartakovskii, a. I.; et al. Light-Emitting Diodes by Band-Structure Engineering in van Der Waals Heterostructures. *Nat. Mater.* **2015**, *14*, 301−306.
(4) Castellanos-Gomez, A.; Roldán, R.; Cappelluti, E.; Buscema, M.; Guinea, F.; Van Der Zant, H. S. J.; Steele, G. A. Local Strain Engineering in Atomically Thin MoS2. *Nano Lett.* **2013**, *13*, 5361.
(5) Desai, S. B.; Seol, G.; Kang, J. S.; Fang, H.; Battaglia, C.; Kapadia, R.; Ager, J. W.; Guo, J.; Javey, A. Strain-Induced Indirect to

Direct Bandgap Transition in Multilayer WSe 2. *Nano Lett.* **2014**, *14* (8), 4592−4597.

(6) Martín-Sánchez, J.; Trotta, R.; Mariscal, A.; Serna, R.; Piredda, G.; Stroj, S.; Edlinger, J.; Schimpf, C.; Aberl, J.; Lettner, T. Strain-Tuning of the Optical Properties of Semiconductor Nanomaterials by Integration onto Piezoelectric Actuators. *Semicond. Sci. Technol.* **2018**, *33* (1), 013001.

(7) Island, J. O.; Kuc, A.; Diependaal, E. H.; Bratschitsch, R.; Van Der Zant, H. S. J.; Heine, T.; Castellanos-Gomez, A. Precise and Reversible Band Gap Tuning in Single-Layer MoSe2 by Uniaxial Strain. *Nanoscale* **2016**, *8* (5), 2589−2593.

(8) Niehues, I.; Schmidt, R.; Drüppel, M.; Marauhn, P.; Christiansen, D.; Selig, M.; Berghäuser, G.; Wigger, D.; Schneider, R.; Braasch, L.; et al. Strain Control of Exciton−Phonon Coupling in Atomically Thin Semiconductors. *Nano Lett.* **2018**, *18* (3), 1751−1757.

(9) Kumar, S.; Kaczmarczyk, A.; Gerardot, B. D. Strain-Induced Spatial and Spectral Isolation of Quantum Emitters in Mono- and Bilayer WSe2. *Nano Lett.* **2015**, *15* (11), 7567−7573.

(10) Aharonovich, I.; Englund, D.; Toth, M. Solid-State Single-Photon Emitters. *Nat. Photonics* **2016**, *10* (10), 631−641.

(11) Tonndorf, P.; Schmidt, R.; Schneider, R.; Kern, J.; Buscema, M.; Steele, G. a.; Castellanos-Gomez, A.; van der Zant, H. S. J.; Michaelis de Vasconcellos, S.; Bratschitsch, R. Single-Photon Emission from Localized Excitons in an Atomically Thin Semiconductor. *Optica* **2015**, *2* (4), 347.

(12) Srivastava, A.; Sidler, M.; Allain, A. V.; Lembke, D. S.; Kis, A.; Imamoğlu, A. Optically Active Quantum Dots in Monolayer WSe2. *Nat. Nanotechnol.* **2015**, *10* (6), 491−496.

(13) He, Y.-M.; Clark, G.; Schaibley, J. R.; He, Y.; Chen, M.-C.; Wei, Y.-J.; Ding, X.; Zhang, Q.; Yao, W.; Xu, X.; et al. Single Quantum Emitters in Monolayer Semiconductors. *Nat. Nanotechnol.* **2015**, *10* (6), 497−502.

(14) Koperski, M.; Nogajewski, K.; Arora, A.; Cherkez, V.; Mallet, P.; Veuillen, J.-Y.; Marcus, J.; Kossacki, P.; Potemski, M. Single Photon Emitters in Exfoliated WSe2 Structures. *Nat. Nanotechnol.* **2015**, *10* (6), 503−506.

(15) Chakraborty, C.; Kinnischtzke, L.; Goodfellow, K. M.; Beams, R.; Vamivakas, a. N. Voltage-Controlled Quantum Light from an Atomically Thin Semiconductor. *Nat. Nanotechnol.* **2015**, *10* (6), 507−511.

(16) Tran, T. T.; Bray, K.; Ford, M. J.; Toth, M.; Aharonovich, I. Quantum Emission from Hexagonal Boron Nitride Monolayers. *Nat. Nanotechnol.* **2016**, *11* (1), 37−41.

(17) Zheng, Y. J.; Chen, Y.; Huang, Y. L.; Gogoi, P. K.; Li, M.-Y.; Li, L.-J.; Trevisanutto, P. E.; Wang, Q.; Pennycook, S. J.; Wee, A. T. S.; et al. Point Defects and Localized Excitons in 2D WSe 2. *ACS Nano* **2019**, *13* (5), 6050−6059.

(18) Chirolli, L.; Prada, E.; Guinea, F.; Roldán, R.; San-Jose, P. Strain-Induced Bound States in Transition-Metal Dichalcogenide Bubbles. *2D Mater.* **2019**, *6* (2), 25010.

(19) Branny, A.; Kumar, S.; Proux, R.; Gerardot, B. D. Deterministic Strain-Induced Arrays of Quantum Emitters in a Two-Dimensional Semiconductor. *Nat. Commun.* **2017**, *8* (May), 1−7.

(20) Palacios-Berraquero, C.; Kara, D. M.; Montblanch, A. R. P.; Barbone, M.; Latawiec, P.; Yoon, D.; Ott, A. K.; Loncar, M.; Ferrari, A. C.; Atatüre, M. Large-Scale Quantum-Emitter Arrays in Atomically Thin Semiconductors. *Nat. Commun.* **2017**, *8* (May), 1−6.

(21) Kern, J.; Niehues, I.; Tonndorf, P.; Schmidt, R.; Wigger, D.; Schneider, R.; Stiehm, T.; Michaelis de Vasconcellos, S.; Reiter, D. E.; Kuhn, T.; et al. Nanoscale Positioning of Single-Photon Emitters in Atomically Thin WSe2. *Adv. Mater.* **2016**, *28*, 7101−7105.

(22) Tripathi, L. N.; Iff, O.; Betzold, S.; Emmerling, M.; Moon, K.; Lee, Y. J.; Kwon, S.-H.; Höfling, S.; Schneider, C. Spontaneous Emission Enhancement in Strain-Induced WSe2Monolayer Based Quantum Light Sources on Metallic Surfaces. *ACS Photonics* **2018**, *5* (5), 1919−1926.

(23) Iff, O.; Lundt, N.; Betzold, S.; Tripathi, L. N.; Emmerling, M.; Tongay, S.; Lee, Y. J.; Kwon, S.-H.; Höfling, S.; Schneider, C.

Deterministic Coupling of Quantum Emitters in WSe 2 Monolayers to Plasmonic Nanocavities. *Opt. Express* **2018**, *26* (20), 25944.

(24) Cai, T.; Kim, J.; Yang, Z.; Dutta, S.; Aghaeimeibodi, S.; Waks, E. Radiative Enhancement of Single Quantum Emitters in WSe2Monolayers Using Site-Controlled Metallic Nanopillars. *ACS Photonics* **2018**, *5*, 3466−3471.

(25) Luo, Y.; Shepard, G. D.; Ardelean, J. V.; Rhodes, D. A.; Kim, B.; Barmak, K.; Hone, J. C.; Strauf, S. Deterministic Coupling of Site-Controlled Quantum Emitters in Monolayer WSe2 to Plasmonic Nanocavities. *Nat. Nanotechnol.* **2018**, *13* (12), 1137.

(26) Chen, H.; Nanz, S.; Abass, A.; Yan, J.; Gao, T.; Choi, D.-Y.; Kivshar, Y. S.; Rockstuhl, C.; Neshev, D. N. Enhanced Directional Emission from Monolayer WSe2 Integrated onto a Multiresonant Silicon-Based Photonic Structure. *ACS Photonics* **2017**, *4*, 3031.

(27) Hartwig, O.; Kaniber, M.; Finley, J. J.; Prechtl, M.; Cerne, J.; Vest, G.; Jürgensen, M.; Blauth, M. Coupling Single Photons from Discrete Quantum Emitters in WSe 2 to Lithographically Defined Plasmonic Slot Waveguides. *Nano Lett.* **2018**, *18* (11), 6812−6819.

(28) Trotta, R.; Martín-Sánchez, J.; Wildmann, J. S.; Piredda, G.; Reindl, M.; Schimpf, C.; Zallo, E.; Stroj, S.; Edlinger, J.; Rastelli, A. Wavelength-Tunable Sources of Entangled Photons Interfaced with Atomic Vapours. *Nat. Commun.* **2016**, *7*, 10375.

(29) Huang, H.; Trotta, R.; Huo, Y.; Lettner, T.; Wildmann, J. S.; Martín-Sánchez, J.; Huber, D.; Reindl, M.; Zhang, J.; Zallo, E.; et al. Electrically-Pumped Wavelength-Tunable GaAs Quantum Dots Interfaced with Rubidium Atoms. *ACS Photonics* **2017**, *4* (4), 868−872.

(30) Grosso, G.; Moon, H.; Lienhard, B.; Ali, S.; Efetov, D. K.; Furchi, M. M.; Jarillo-Herrero, P.; Ford, M. J.; Aharonovich, I.; Englund, D. Tunable and High-Purity Room Temperature Single-Photon Emission from Atomic Defects in Hexagonal Boron Nitride. *Nat. Commun.* **2017**, *8* (1), 705.

(31) Castellanos-Gomez, A.; Buscema, M.; Molenaar, R.; Singh, V.; Janssen, L.; van der Zant, H. S. J.; Steele, G. a. Deterministic Transfer of Two-Dimensional Materials by All-Dry Viscoelastic Stamping. *2D Mater.* **2014**, *1* (1), 011002.

(32) Trotta, R.; Atkinson, P.; Plumhof, J. D.; Zallo, E.; Rezaev, R. O.; Kumar, S.; Baunack, S.; Schröter, J. R.; Rastelli, A.; Schmidt, O. G. Nanomembrane Quantum-Light-Emitting Diodes Integrated onto Piezoelectric Actuators. *Adv. Mater.* **2012**, *24* (20), 2668−2672.

(33) Regelman, D. V.; Mizrahi, U.; Gershoni, D.; Ehrenfreund, E.; Schoenfeld, W. V.; Petroff, P. M. Semiconductor Quantum Dot: A Quantum Light Source of Multicolor Photons with Tunable Statistics. *Phys. Rev. Lett.* **2001**, *87*, 257401.

(34) Zhang, J.; Wildmann, J. S.; Ding, F.; Trotta, R.; Huo, Y.; Zallo, E.; Huber, D.; Rastelli, A.; Schmidt, O. G. High Yield and Ultrafast Sources of Electrically Triggered Entangled-Photon Pairs Based on Strain-Tunable Quantum Dots. *Nat. Commun.* **2015**, *6*, 1−7.

(35) He, Y.-M.; Iff, O.; Lundt, N.; Baumann, V.; Davanco, M.; Srinivasan, K.; Hofling, S.; Schneider, C. Cascaded Emission of Single Photons from the Biexciton in Monolayered WSe₂. *Nat. Commun.* **2016**, *7*, 13409.

(36) Martín-Sánchez, J.; Trotta, R.; Piredda, G.; Schimpf, C.; Trevisi, G.; Seravalli, L.; Frigeri, P.; Stroj, S.; Lettner, T.; Reindl, M. Reversible Control of In-Plane Elastic Stress Tensor in Nanomembranes. *Adv. Opt. Mater.* **2016**, *4* (5), 682.

(37) Martín-Sánchez, J.; Mariscal, A.; De Luca, M.; Martín-Luengo, A. T.; Gramse, G.; Halilovic, A.; Serna, R.; Bonanni, A.; Zardo, I.; Trotta, R.; et al. Effects of Dielectric Stoichiometry on the Photoluminescence Properties of Encapsulated WSe2Monolayers. *Nano Res.* **2018**, *11*, 1399.